Chin.J.Geochem.(2014)33:289–299
DOI: 10.1007/s11631-014-0690-2

Research on the inversion of elemental abundances from Chang'E-2 X-ray spectrometry data

BAN Chao[1,2], ZHENG Yongchun[1,3*], ZHU Yongchao[1,2], ZHANG Feng[1,2], XU Lin[1], and ZOU Yongliao[1**]

[1] *National Astronomical Observatories, Chinese Academy of Sciences, Beijing 100012, China*

[2] *University of Chinese Academy of Sciences, Beijing 100049, China*

[3] *Space Science Institute, Macau University of Science and Technology, Macau, China*

[*] *Corresponding author, E-mail: zyc@nao.cas.cn*

[**] *Corresponding author, E-mail: ylzou@nao.cas.cn*

Received August 24, 2013; accepted November 15, 2013

Abstract The elemental abundances of lunar surface are the important clues to study the formation and evolution history of the Moon. In 2010, China's Chang'E-2 (CE-2) lunar orbiter carried a set of X-ray spectrometer (XRS) to investigate the elemental abundances of the lunar surface. During CE-2's life span around the Moon, the XRS experienced several events of solar flare. The X-ray solar monitor onboard recorded the spectra of solar X-rays at the same time. In this paper, we introduced the XRS instrument and data product. We analyzed the characteristics of the XRS data. Using the data obtained during an M solar flare event which had occurred on Feb. 16, 2011, we derived the elemental abundances of Mg, Al, Si, Ca and Fe of the lunar surface in the Oceanus Procellarum. Finally, we discussed the factors that influence the accuracy of the inversion.

Key words Chang'E-2;X-ray spectrometer; elemental abundance; lunar surface; Moon

1 Introduction

The information about the chemical composition of the lunar surface (elements, minerals and rocks) is an important clue to study the origin and evolution of the Moon. Almost every lunar mission, including unmanned and manned lunar missions, carried out the survey of lunar surface composition. In-orbit remote measurements in gamma-ray, X-ray, visible and near-IR wavelengths were the major methods adopted by the missions. Larger region-wide elemental abundance distributions could be mapped with less expense by employing those techniques.

The X-ray fluorescence of lunar-surface elements which does not emit spontaneously is mainly excited by solar X-ray. By detecting the characteristic X-ray fluorescence spectra, the elemental abundances of the lunar surface (Mg, Al, Si, Ca, Ti, Fe and other major elements) could be obtained via an inversion method. The elemental abundances derived from X-ray fluorescence could be compared to those derived from gamma-ray and other spectral techniques, and the results obtained by various measurements could also be compared and complemented each other.

Apollo 15 and 16, respectively lunched in 1972 and 1973, detected elemental X-ray fluorescence in the lunar orbit for the first time, and mapped Mg/Si and Al/Si abundance ratios distribution over an area accounting for about 10% of the Moon (Adler et al., 1972; Adler et al., 1973a; Adler et al., 1973b). In 2003, SMART-1 lunched by Europe was equipped with a D-CIXS (the demonstration of compact imaging X-ray spectrometer) detector. SMART-1 crossed Earth's radiation belts for many times on the way to the Moon and D-CIXS suffered proton radiation damage, so that accurate quantitative study has not been carried out (Narendranath et al., 2011). The X-ray spectrometer mounted on Japanese first lunar satellite SELENE also suffered the radiation damage, resulting in the reduced ability of detection (Okada et al., 2009). An X-ray spectrometer carried by Chang'E-1 (CE-1) which was launched by China in 2007, and C1XS (Chandrayyan-1 X-ray spectrometer) equipped on Chandrayyan-1 which was launched by India in 2008, both obtained a little data. As the Sun was in a quiet period and solar flare occurred only a few times, only a small region-wide elemental abundances distribution was mapped for each of the two missions.

The X-ray spectrometer on Chang'E-2 (CE-2) which was launched in 2010, was an improved instrument compared to the original one that was

equipped on CE-1. The X-ray solar monitor on the X-ray spectrometer could simultaneously get the spectra of solar X-rays. During the CE-2 mission, the Sun was in an active period and a great deal of solar flare occurred, which makes it possible to map abundances distribution of major elements in the lunar surface.

2 Instrument and data

2.1 X-ray spectrometer (XRS)

XRS onboard CE-2 and the one equipped on CE-1 have similar structures. Both of them were composed of X-ray fluorescence spectrometer (XRF), X-ray solar monitor (XSM) and electronics chassis. XRF and XSM respectively detected X-ray fluorescence signals from major elements of the lunar surface and the spectra of solar X-rays.

The X-ray fluorescence signals from lunar-surface major elements detected by XRF were excited by solar X-ray. In that case the intensity of X-ray fluorescence from the lunar surface is closely related to that of solar X-ray. The spectra of solar X-ray obtained by XSM are necessary for the inversion of elemental abundances.

XRF has four Si-PIN detectors with 1024 channels for each one. The energy range of detection was 0.6–10.6 keV; energy resolution was 300 eV at 5.95 keV and effective detection area of each detector was 1 cm^2. XRF integrated the events of X-ray fluorescence with a 50 s period. In this paper, the events of X-ray fluorescence in two periods (100s) were accumulated to enhance statistics. XRS carried a ^{55}Fe radioactive calibration source which yielded a characteristic X-ray line at 5.9 keV. The X-ray line emitted by ^{55}Fe which was detected by XRF could be used for calibration in the orbit.

XSM used a Si-PIN detector with 976 channels and a 12.5 μm Be window. The energy range of detection was 0.6–10.7 keV; energy resolution was 300 eV at 5.95 keV and the detection area of the detector was 25 cm^2. To avoid the count rate of XSM data acquisition system from reaching the saturation value (3300 counts per second) easily, a copper cap was fixed in the front of the Be window with a hole as big as 0.5 mm in diameter in the center. The detection area decreased by 99.2% and the actual effective detection area was 0.2 cm^2. XSM integrated the events of solar X-ray within a 10 s period.

CE-2 was in an orbit at 100km above the lunar surface. At that altitude the instantaneous detection area of XRF on the lunar surface was about 73 km×200 km. The major indicators of XRS are given in Table 1.

Table 1 Major indicators of XRS onboard CE-2

	XRF	XSM
Detector	Si-PIN×4 chips	Si-PIN×1 chips
Incident window	12.5 μm Be	12.5 μm Be
Energy range	0.6–10.6keV	0.6–10.7keV
Effective detection area	1 cm^2	0.2 mm^2
Energy resolution	300 eV@5.95 keV	300 eV@5.95 keV

2.2 Data of XRS

XRS had been operating for about 7 months since it was powered up on October 15, 2010. During the XRS operation, its status is shown in Table 2. According to the temperature of XRS, ephemeris data and satellite attitude data, XRS was judged to be in normal operation condition.

Not all detection data acquired during XRS operating were able to be used to inverse elemental abundances. Only the detection data which were acquired under specific observation conditions can be used. In this paper, the XRS data were selected based on the following principles to test the inversion method and process:

(1) The level of solar flare should be above class C. According to the strength of energy, the levels of solar flare ranging from strong to weak are classified as classes X, M, C, B and A. The more intense the solar flare is, the more elemental X-ray fluorescence can be excited, the more obvious the characteristic X-ray fluorescence lines of elements are, and the higher the fitting precision is. That benefits the inversion of the abundances of major elements.

(2) The count rates of XRF and XSM should not exceed the saturation value (3300 counts per second). The designed saturation values of XRF and XSM count rate were 3300 counts per second. The count rate was 0 or negative for each channel of XRF and XSM, when the rate exceeded that threshold.

(3) The solar X-ray incident angle of the observed point should be less than 90°, which means XRS on the sunlit side. The X-ray fluorescence of lunar-surface elements is excited by solar X-ray except radioactive elements. XRS was on the dark side when the solar X-ray incident angle was greater than 90°.

(4) The solar X-ray incident angle of XSM (the angle between solar X-ray incident direction and XSM optical axis) should be less than 60°. XSM was designed not to carry out angle correction of the data acquired when solar X-ray incident angle was greater than 60°. If the data with no angle correction are used, a great error will exist.

(5) The detection data from a mare area should be chosen. The abundances of Ti and Fe are generally

higher in the mare area than in the highland area, so the characteristic X-ray lines of the two elements are more obvious. That is beneficial for the inversion of Ti and Fe elemental abundances.

Based on the above principles, the data at 9:06:36 to 9:15:46 on February 16, 2011 were selected in this paper to analyze the abundances of elements on the surface of the Moon. As the GOES satellite showed that a class-M solar flare occurred during the selected time (http://www.swpc.noaa.gov/ftpmenu/warehouse/2011/2011_plots. html), and XSM captured that event. The detection area is located at the Oceanus Procellarum (12.8°–38.2° N, 50° W) during the solar flare (Fig. 1).

After the raw data were obtained by XRS, they were transmitted through an antenna on CE-2 to the system on the ground. The data were processed to 2C level data by the Lunar Exploring Ground Application System at the National Astronomical Observatories. Steps of data processing are shown in Fig. 2.

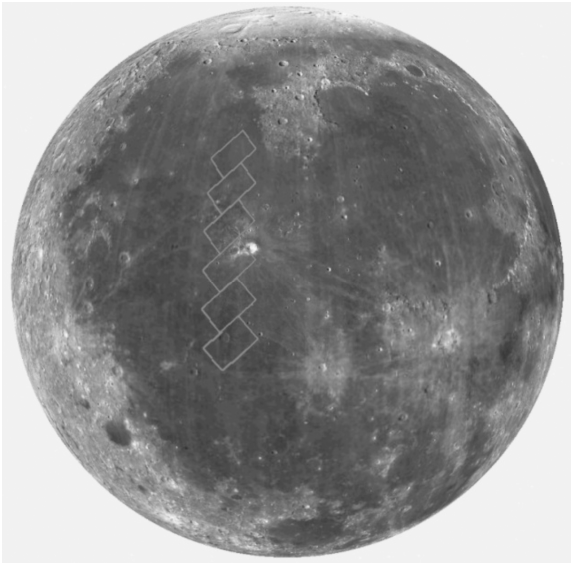

Fig. 1. The observed region in this paper.

3 Analysis of XRS data

3.1 XRF background spectrum

A continuum background spectrum was detected by XRF in the lunar orbit. The average count rate for each detector was about 1.3 counts per second. The background spectrum resulted from two sources. The internal one was electronic noise generated during XRF operating. The external one refers to the existence of high energy particles in space environment and scattered X-rays from the Moon. These sources resulted in energy deposition in the detectors of XRF, thereby the detectors forming X-ray fluorescence counts that were the background spectra. By analyzing the XRF background spectra, XRF spectrum processing could be optimized.

Table 2 The status of XRS during its operation

Time	Status
2010-10-15 15:27:24－2010-10-23 19:04:36	on
2010-10-23 19:04:36－2010-11-01 01:08:12	off
2010-11-01 01:08:12－2010-11-30 06:06:22	on
2010-11-30 06:06:22－2010-11-30 13:15:10	off
2010-11-30 13:15:10－2010-12-20 22:06:00	on
2010-12-20 22:06:00－2010-12-24 20:53:24	off
2010-12-24 20:53:24－2011-01-20 19:50:51	on
2011-01-20 19:50:51－2011-01-24 03:46:39	off
2011-01-24 03:46:39－2011-04-13 19:13:06	on
2011-04-13 19:13:06－2011-04-15 23:27:59	off
2011-04-15 23:27:59－2011-04-23 08:27:35	on
2011-04-23 08:27:35－2011-04-25 09:04:52	off
2011-04-25 09:04:52－2011-05-12 16:37:52	on
2011-05-12 16:37:52－2011-05-12 18:42:51	off
2011-05-12 18:42:51－2011-05-20 20:00:00	on
2011-05-20 20:00:00－Fly away from the Moon	off

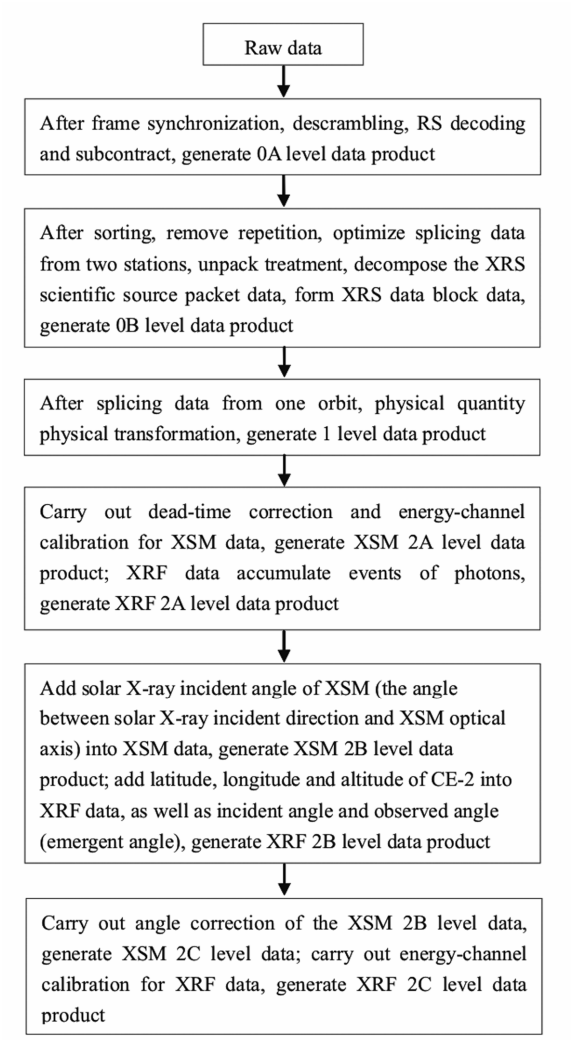

Fig. 2. Steps involved in XRS data processing from raw data to 2C level.

The temperature of XRF changed within an orbit. Shown in Fig. 3 is the effect of temperature on XRF background spectra, suggesting that there is no temperature dependence for the background spectra. So, the effect of temperature variation on the background spectra is supposed to be negligible.

There are many particles in the orbit (lunar gamma-ray, solar radiation, cosmic ray, etc.). As the upper limit of XRF detection energy was 10.6 keV, the particles with energy being less than 10.6 keV detected by XRF may form counts in the detectors. The particles with energy being greater than 10.6 keV may interact with the material of XRF and other particles surrounding the detectors to generate lower energy particles which then deposited the energy in the detectors. The counts are mainly within 3keV, which suggests that lower energy particles make large contributions to the XRF background spectra. In Fig.3, there is a ^{55}Fe characteristic X-ray line at 5.9 keV. That is because XRS was equipped with a ^{55}Fe radioactive calibration source (if there is no special instruction in this paper, the characteristic line at 5.9 keV should be due to ^{55}Fe).

As the characteristic X-ray fluorescence lines of lunar-surface elements were detected on the sunlit side, it is necessary to analyze the XRF background spectrum generated when XRF was on the sunlit side. Background spectra from both sunlit side and dark side are compared with each other, as shown in Fig. 4, and they are found to be very similar. This suggests the space environment is of no significant difference between the sunlit side and the dark side and scattered X-ray from the lunar surface was very weak at quiet solar conditions.

3.2 Analysis of X-ray fluorescence spectrum

XRF was on the sunlit side during the M solar flare and moved to the dark side when the solar flare approached to the end. XRF detected the characteristic X-ray fluorescence lines of Mg, Al, Si, Ca, Ti and Fe. Shown in Fig. 5 is the comparison of X-ray fluorescence spectra detected on the sunlit side and the background spectra obtained by XRF when on the dark side in the same orbit. X-ray fluorescence spectra in Fig.5 indicate the count rates during the whole process of the solar flare. The characteristic X-ray fluorescence line of Ti is shown in Fig. 5. But for each detection period the counts of X-ray fluorescence of Ti were so few that its characteristic line could not form. Sometimes the characteristic line of Ti might be detected, however, there will be involved a great error in the calculation of X-ray fluorescence intensity of Ti because of the low statistics. Therefore, the elemental abundances of Mg, Al, Si, Ca and Fe were inversed during that solar flare. After the obtained XRF background spectrum was subtracted, X-ray fluorescence spectrum in each detection period was fitted with a model consisting of a Gaussian function for the elemental characteristic X-ray fluorescence lines and a scattered solar spectral model for the residual continuous spectrum (shown in Fig. 6). According to the fittings, elemental intensities in each detection period are given in Table 3.

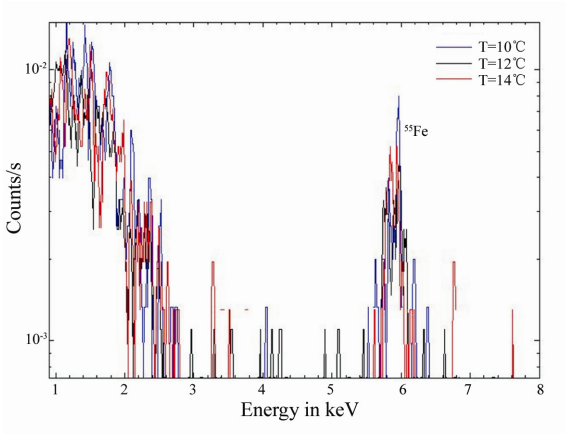

Fig. 3. XRF background spectra at different temperatures. Solid lines in blue, black and red respectively represent the background spectra at 10, 12 and 14℃. The similarity of different background spectra indicates that the effect of temperature variation is negligible.

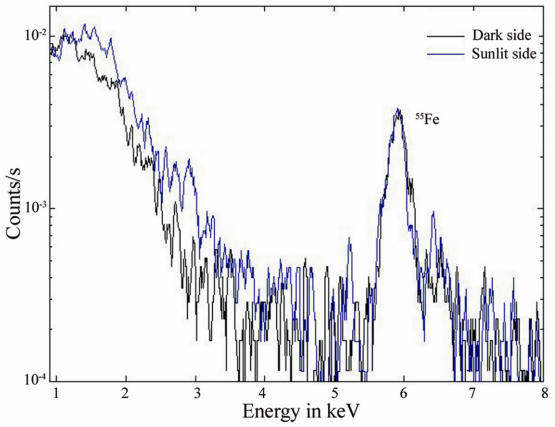

Fig. 4. Comparison of XRF background spectra detected on both sunlit side (blue solid line) and dark side (black solid line). It is found that both of them are very similar.

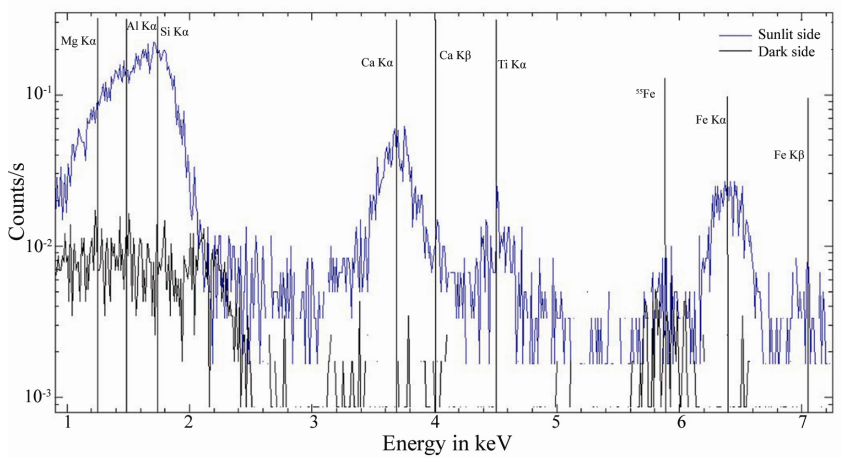

Fig. 5. X-ray fluorescence spectra (blue solid line) on the sunlit side and background spectra (black solid line) on the dark side.

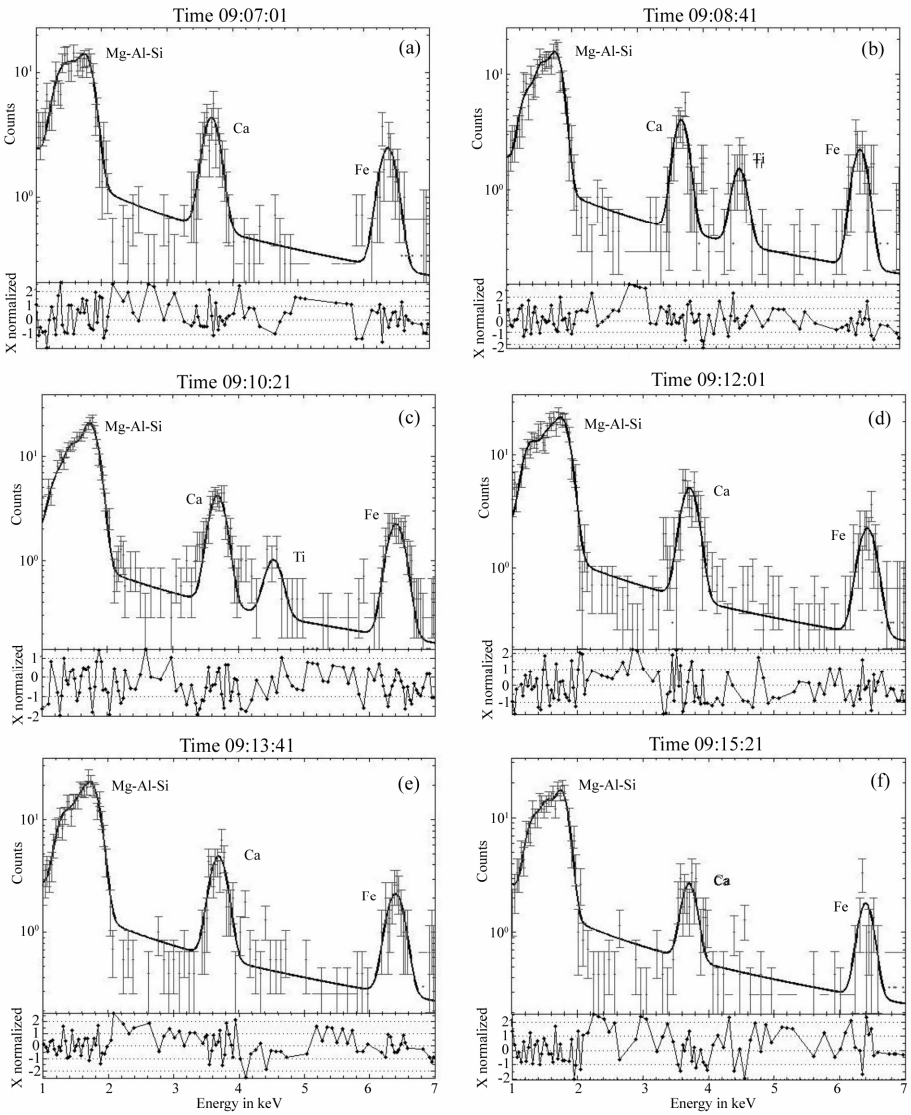

Fig. 6. Fittings of X-ray fluorescence spectra for each detection period (from a to f) during the M solar flare. A detection period is 100s. Fitting residuals (the ratio of the difference between fitting result and measurement data to measurement error) are shown at the bottom. The elemental characteristic line of Ti is seen in b and c, but Ti elemental abundance is not inversed in any period because of the low statistics.

Table 3 Elemental intensities acquired in each detection period with 2σ errors during the M solar flare. The latitudes and longitudes of the observed region are the coordinates of CE-2

Time	Latitude	Longitude	Mg Kα	Al Kα	Si Kα	Ca Kα	Fe Kα
09:07:01	12.8°	-48.6°	160.6±30.8	189.3±38.7	296.4±26.4	97.45±15.45	36.22±5.11
09:08:41	17.9°	-48.8°	133.4±37.1	158.5±34.8	325.3±29.8	73.48±11.16	38.00±2.91
09:10:21	23.0°	-49.1°	204.4±52.9	252.1±38.3	464.1±43.7	94.92±17.28	55.72±15.75
09:12:01	28.1°	-49.3°	240.4±32.1	256.1±38.5	493.1±30.2	117.1±18.6	53.10±4.72
09:13:41	33.1°	-49.7°	170.8±37.7	216.3±34.7	441.6±39.8	106.0±16.35	33.41±12.17
09:15:21	38.2°	-49.9°	154.1±47.2	175.2±29.5	382.6±19.4	78.21±9.27	16.97±7.18

3.3 Analysis of solar X-ray intensity

X-ray fluorescence of lunar-surface elements is excited by solar X-ray. The X-ray fluorescence intensities of lunar-surface elements detected by XRF are proportional to those of incident solar X-ray and lunar-surface elemental abundances. Therefore, lunar-surface elemental abundances are determined both by the intensity of incident solar X-ray and by the X-ray fluorescence intensities of lunar-surface elements. Both of the intensities are crucial for the inversion of elemental abundances.

The intensity of solar X-ray is obtained by fitting solar X-ray spectrum detected by XSM during each detection period. Shown in Fig. 7 is one of the fittings of solar X-ray spectra gained in the peak phase of the M flare. The emission line of Fe XXV is seen at 6.7keV and is used for calibration in the orbit (during XSM operating, the parameters for the function which maps the number of detector's channels to energy might change with the temperature). After calibration, the intensity of solar X-ray is obtained by using a single temperature model to fit solar X-ray spectrum (Peng, 2009). The intensity of solar X-ray in each period could be acquired by this method.

4 Method and results

4.1 Method of inversion

For any sample, the method of calculating X-ray fluorescence intensities for elements has been widely used in various laboratories. As synchronous incident X-ray is often lacked for observations of planets, this method could not be used directly. Elemental abundances obtained in the past were derived from the ratios of observed elemental X-ray fluorescence intensities to theoretical calculation intensities of the samples.

Apollo 15 and 16 used solar X-ray flux from Solrad 10 satellite to build a two -temperature model. In that model the emission measurement ratio (EMR) -- the ratio of the temperature of solar active spot to the temperature of quiet corona -- represents the change of solar X-ray (Clark et al., 1997; Peng, 2009). In the case of EMR=0.03, the theoretical intensities of elemental X-ray fluorescence were calculated by using the fundamental parameter method, and then the relationship between the ratio of theoretical intensities and the ratio of elemental abundances was obtained. A correction factor was defined as a function of EMR. The ratio of observed intensities in EMR=0.03 was obtained by the ratio in other EMR multiplying the correction factor, then the ratio of elemental abundances was gained (Adler et al., 1972). This method was adopted by CE-1 XRS by using GOES satellite. The XSM onboard CE-2 could detect solar X-ray spectra and the upper limit of its energy is 10.7keV. The intensity of solar X-ray was obtained by fitting. In this paper, the difference with the method adopted by Apollo is that the fundamental parameter method was directly implemented to derive absolute elemental abundances from the intensities of elemental X-ray fluorescence.

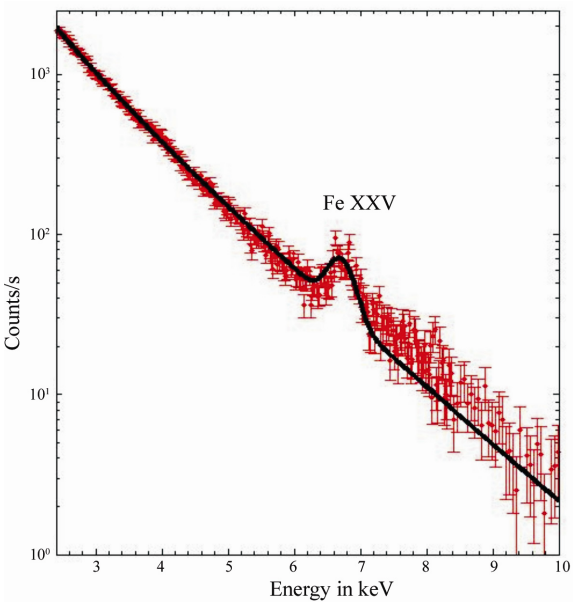

Fig. 7. Solar X-ray spectrum detected by XSM in the peak phase of the M solar flare and fitted by a single temperature model. The emission line of Fe XXV was used for calibration in the orbit.

For a known incident X-ray, the intensities of elemental X-ray fluorescence given off by any known sample can be calculated by a formula (Sherman, 1955; Shirawai and Fujino, 1966; Clark et al., 1997). Secondary X-ray fluorescence will gives rise to the significant enhance of effect, tertiary X-ray fluorescence has only a little effect (Shirawai and Fujino, 1966; Ji Anget al., 2003). In addition to X-ray fluorescence, incident X-ray also interacts with the sample and generates Rayleigh and Compton scattering. As the intensities of the two scatterings are very weak, they could be negligible. In this paper, the first and secondary X-ray fluorescences were taken into consideration.

$$S_{\mathrm{j}}=\int_{E_{\min}}^{E_{\max}}\left(P_j+\sum_k S_{jk}\right)de$$

In the above equation, S_{j} is the total X-ray fluorescence intensity for element $_{\mathrm{j}}$, P_{j} is the intensity of the first X-ray fluorescence and $\sum_k S_{\mathrm{jk}}$ is the intensity of the secondary X-ray fluorescence.

For the intensity of the first X-ray fluorescence:

$$P_j=\frac{I_{\mathrm{sun}}E_{\mathrm{j}}}{4\pi}\cdot\frac{C_{\mathrm{j}}\mu_{\mathrm{j}}(E)}{\sum_{\mathrm{i}}C_{\mathrm{i}}[\mu_{\mathrm{i}}(E)\sec\alpha+\mu_{\mathrm{i}}(E)\sec\beta]}$$

where I_{sun} is the intensity of incident solar X-ray, C_{j} is the abundance of element j, $\mu_{\mathrm{j}}(E)$ is the mass absorption coefficient of element j, α is the angle of incidence, β is the angle of emergence and $\varepsilon j=J_j f_{\mathrm{j}}\omega_{\mathrm{j}}$ is the excitation factor of element j, where $I_{\mathrm{j}}=\frac{r_{\mathrm{k}}-1}{r_{\mathrm{k}}}$ and r_{k} is the k edge jump ratio, f_{j} is the weight fraction and ω_{j} is the fluorescent yield.

For the intensity of secondary X-ray fluorescence:

$$S_{\mathrm{jk}}=P_{\mathrm{j}}\cdot e_{\mathrm{jk}}C_{\mathrm{k}}$$

Where r_{j} is the first X-ray fluorescence of element j, C_{k} is the abundance of element k and $e_{\mathrm{jk}}=[e(e'+e'')]E_{\mathrm{k}}$ where $e=\frac{1}{2}\varepsilon_{\mathrm{k}}\mu_{\mathrm{j}}(E_{\mathrm{k}})\left[\frac{\mu_{\mathrm{k}}(E)}{\mu_{\mathrm{k}}(E)}\right]$, $e'=\frac{1}{\mu'}\ln\left[1+\frac{\mu'}{\mu_{\mathrm{m}}(E_{\mathrm{k}})}\right]$, $e''=\frac{1}{\mu''}\ln\left[1+\frac{\mu''}{\mu_{\mathrm{m}}(E_{\mathrm{k}})}\right]$ and $\mu'=\sum_{\mathrm{i}}C_{\mathrm{i}}\mu_{\mathrm{i}}(E)\sec\alpha$, $\mu''=\sum_{\mathrm{i}}C_{\mathrm{i}}\mu_{\mathrm{i}}(E_{\mathrm{j}})\sec\beta$, $\mu_{\mathrm{m}}(E_{\mathrm{k}})=\sum_{\mathrm{i}}C_{\mathrm{i}}\mu_{\mathrm{i}}(E_{\mathrm{k}})$

Although the intensities of elemental X-ray fluorescence for any known sample can be calculated by a theoretical formula, inversing elemental abundances from the given intensities of elemental X-ray fluorescence is very difficult because of the complexity of that formula. In this paper, X-ray fluorescence intensity fraction (ratio of X-ray fluorescence intensity for an element to the total intensity of X-ray fluorescence) for every element is calculated by the theoretical formula using a set of initial elemental abundances (the average composition of returned samples). By comparing the calculated X-ray fluorescence intensity fraction with the observed one, the initial elemental abundances should be modified. After iterating calculation, the best set of elemental abundances was derived by using the method of least squares. In this way elemental abundances would be acquired from the observed elemental X-ray fluorescence intensities and solar X-ray intensities.

4.2 The preliminary results

The elemental abundances derived from X-ray fluorescence intensities of lunar -surface elements (Table 3) during the M solar flare are listed in Table 4. Element Ti was not taken into calculation in the preliminary inversion. The effect of Ti was discussed in the next section. In this calculation, the sum of abundances of oxides of observed elements (MgO, Al_2O_3, SiO_2, CaO and FeO) was normalized to 100%, so the abundance of element O is determined by the abundances of the observed elements. The angles of incidence and emergence were provided by the detectors on CE-2. For comparison, the results of Lunar Prospector gamma-ray spectrometer (LP GRS) and the average composition of soils from Apollo 11, 12 and Luna 16, 24 are also listed in Table 4.

4.3 Modified results for oxides of other elements

The intensities of X-ray fluorescence of lunar-surface elements are proportional to the abundances of those elements. As CE-2 was working at an altitude of 100km, X-ray fluorescence given off by the elements with low abundances is difficult to detect. Even if they were detected, the X-ray fluorescence intensities of those elements could not be calculated to get a result because of low statistics. In this paper, these elements are not taken into calculation at first, however, these elements have two following effects on the results of calculation: 1) Effect on the percentage of elemental abundance. As there is an assumption in calculation that the sum of abundances of oxides of observed elements (MgO, Al_2O_3, SiO_2, CaO and FeO) was 100%, unobserved elements could lead to a decrease in the calculated abundance of every observed element. 2) Effect of secondary X-ray fluorescence. X-ray fluorescence of unobserved elements could excite secondary X-ray fluorescence of other elements which have less atomic weight. As secondary X-ray

fluorescence was taken into account in this paper, unobserved elements could cause a decrease in calculated abundances of the elements which have less atomic weight.

In this paper, the effects of unobserved elements were analyzed by quantitative calculation. It is known that the abundance of element Ti is generally higher in mare area than in highland. According to the abundance of Ti derived from returned samples and LP GRS, its abundance is highest among other unobserved elements. So, Ti is considered as the main factor to influence the result. The values on the right listed in Table 4 are the results in case that Ti is taken into calculation (the abundance of TiO_2 is fixed at 6.0%, which is the average value derived from LP GRS in this observed region). The sum of abundances of oxides of the 6 elements (MgO, Al_2O_3, SiO_2, CaO, TiO_2 and FeO) are normalized to 100% in the calculation. The effect of Ti on other elements is shown in Table 4, which is within the range of 2σ errors. The abundance of Si decreases much more significantly than the abundances of other elements. The comparison of the first and modified results with the values derived from LP GRS is shown in Fig. 8. Relative to the values derived from LP GRS, the calculated results show that the abundance of Fe is overall high, in the region where the latitude is higher than 25° the abundance of Al is relatively high, but that of Ca is relatively low, while in the region where the latitude is lower than 25°the abundance of Si is relatively high.

In addition to Ti, the abundances of some other elements in lunar soil are greater than 0.01%, X-ray fluorescence of those elements was not detected by XRF on CE-2. The sum of abundances of other elements (except for MgO,Al_2O_3,SiO_2,CaO,TiO_2 and FeO) in the returned samples is 0.97%–2.31% (McKay et al., 1991; Ouyang Ziyuan et al., 2005), which is much smaller than the value of TiO_2, so its effect on the calculated results is much less.

5 Discussion

5.1 The effect of lunar soil grain size on the calculated results

Laboratory experiments have indicated that the grain size has effect on the intensity of elemental X-ray fluorescence:

(1) For a given element, its X-ray fluorescence intensity decreases with increasing particle size and the extent of decrease varies with different elements (Maruyama et al., 2008; Naranen et al., 2008). Some experiments have shown that the effect of grain size on the elemental X-ray fluorescence intensity is within the range of 10% (Okada and Kuwada, 1997). The 2σ errors of calculated results are about 10% or more (Table 4), so the extent of the effect is equal to or less than the calculated error.

Table 4 Elemental abundances (%) with 2σ errors for each observed period during the M solar flare

Time	Latitude	Longitude	Mg*		Al*		Si*		Ca*		Fe*	
09:07:01	12.8°	-48.6°	8.5	+2.0 -2.0	8.0	+1.9 -1.9	9.9	+1.9 -2.0	9.2	+1.8 -1.9	15.0	+1.9 -1.9	13.9	+1.8 -1.8	6.8	+1.9 -1.9	6.2	+1.8 -1.8	19.8	+2.2 -2.7	19.4	+2.1 -2.5
09:08:41	17.9°	-48.8°	7.3	+1.6 -1.6	6.8	+1.5 -1.5	8.4	+1.5 -1.6	7.8	+1.5 -1.5	16.8	+1.5 -1.5	15.4	+1.4 -1.4	5.2	+1.5 -1.5	4.8	+1.4 -1.4	22.4	+1.7 -2.0	21.9	+1.6 -1.9
09:10:21	23.0°	-49.1°	7.8	+1.6 -1.7	7.4	+1.5 -1.6	9.5	+1.6 -1.6	8.9	+1.5 -1.5	17.1	+1.5 -1.5	15.8	+1.5 -1.5	6.5	+1.5 -1.5	6.0	+1.5 -1.5	18.1	+1.8 -2.1	17.8	+1.7 -2.0
09:12:01	28.1°	-49.3°	8.6	+1.4 -1.5	8.2	+1.3 -1.4	9.2	+1.4 -1.4	8.6	+1.3 -1.3	17.2	+1.4 -1.4	15.9	+1.3 -1.3	5.6	+1.4 -1.4	5.2	+1.3 -1.3	18.3	+1.6 -1.8	18.0	+1.5 -1.7
09:13:41	33.1°	-49.7°	7.0	+2.0 -2.0	6.6	+1.9 -1.9	8.9	+2.0 -2.0	8.4	+1.9 -1.9	18.3	+1.9 -1.9	16.8	+1.8 -1.8	7.0	+1.9 -1.9	6.5	+1.8 -1.8	17.5	+2.3 -2.8	17.2	+2.2 -2.6
09:15:21	38.2°	-49.9°	7.0	+1.9 -2.0	6.6	+1.8 -1.8	8.2	+1.9 -1.9	7.7	+1.8 -1.8	18.5	+1.9 -1.9	17.1	+1.8 -1.7	7.8	+1.8 -1.9	7.2	+1.7 -1.8	17.4	+2.3 -2.8	17.1	+2.2 -2.5
Apollo 11	0°41.4′	23°25.8′	4.7		7.2		19.7		8.5		11.9	
Apollo 12	-2°27′	-23°20.4′	5.6		6.8		21.9		7.6		11.7	
Luna 16	-0°41′	56°18′	5.3		8.1		20.0		8.9		13.0	
Luna 24	12°15′	62°12′	5.7		6.6		20.5		8.8		15.4	
LP	7.5°–12.5°	-45°—-50°	8.0		5.9		14.9		8.3		18.5	
	12.5°–17.5°	-45°—-50°	8.7		9.4		12.8		6.5		17.1	
	17.5°–22.5°	-45°—-50°	9.0		7.8		13.2		6.4		19.0	
	22.5°–27.5°	-45°—-50°	9.4		9.2		13.2		6.4		17.1	
	27.5°–32.5°	-45°—-50°	9.3		4.6		16.7		8.3		16.6	
	32.5°–37.5°	-48°—-54°	8.2		7.2		17.0		7.8		15.6	
	37.5°–42.5°	-48°—-54°	7.1		5.8		17.5		9.8		15.3	

*: Values on the left are the results with TiO_2 being excluded and values on the right are the results with TiO_2 being taken into calculation. The effect of TiO_2 was discussed in the next section. The average composition of soils from Apollo 11, 12 and Luna 16, 24 and the results of LP GRS are listed in the table. Latitudes and longitudes of the observed regions are the coordinates of CE-2. Latitudes and longitudes of Apollo 11, 12 and Luna 16, 24 are the coordinates of the sites of landing.

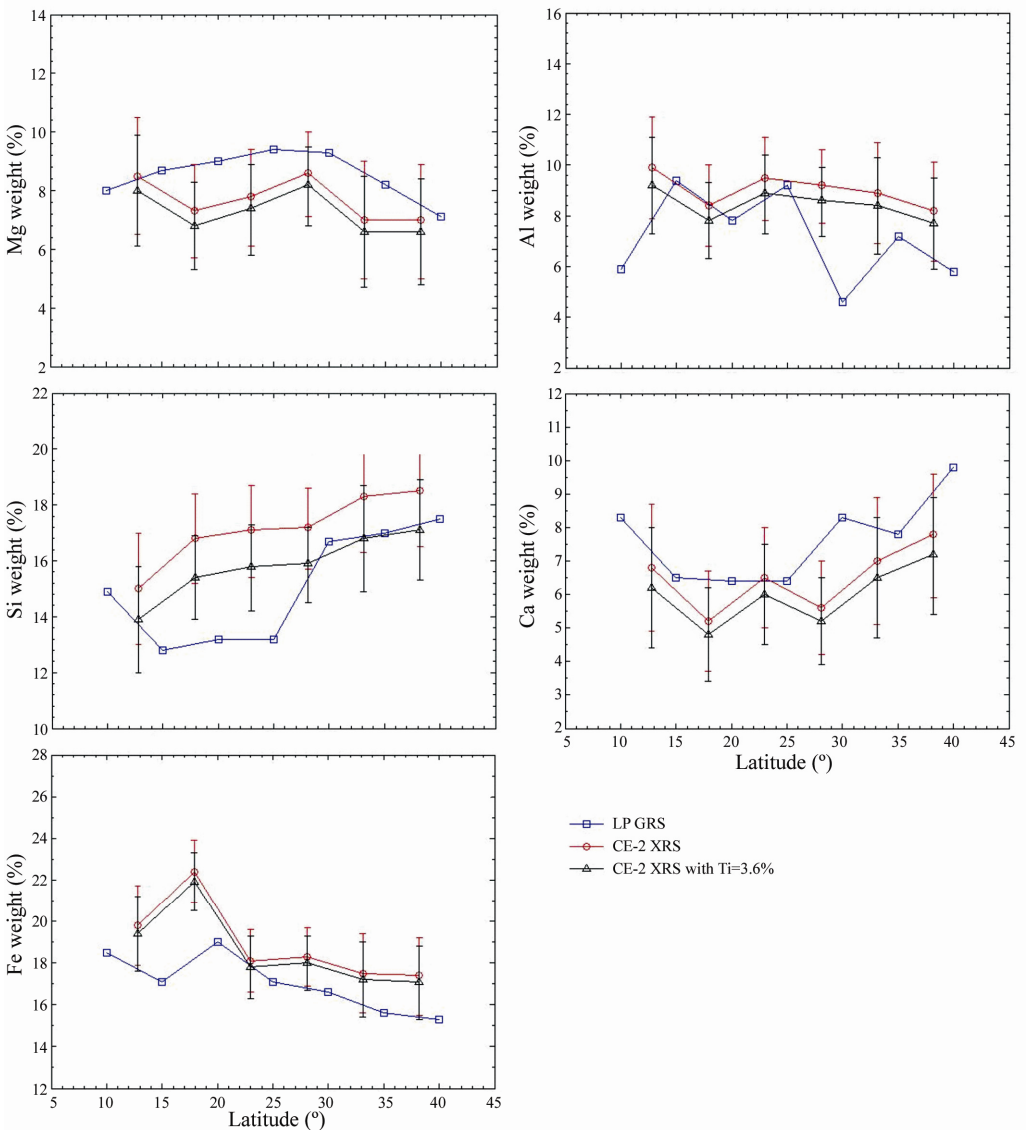

Fig. 8. Comparison of the first results (red solid line) and modified results (black solid line) derived from XRS on CE-2 with the results derived from LP GRS (blue solid line). After the abundance of TiO_2 (6.0%) was taken into account, the abundances of all elements tend to decrease.

(2) The intensity of elemental X-ray fluorescence has correlations with the angle of incident solar X-ray and the phase angle (the angle between incident angle and emergent angle). For a given grain size, the intensity of elemental X-ray fluorescence varies with different incident angles or phase angles. The difference of intensity decreases with decreasing grain size (Okada, 2004; Naranen, et al., 2007, 2008, 2009).

(3) Different elements are concentrated in different minerals. If the grain size is larger than the mean free path of X-ray, this would affect the intensity of elemental X-ray fluorescence (Nittler et al., 2001). It is suggested that this effect is negligible in case the grain size decreases (Narendranath et al., 2011).

In addition, in laboratory experiments Apollo 16 Clam Shell Sampling Devices (CSSDs) were adopted to analyze soils from the top 100 and 500 μm of the soil. It is suggested that ultrafine (<2 μm) particles dominate the uppermost lunar surface (Noble, 2010). As the grains less than 2 μm account for a higher proportion, the effect of lunar soil grain size will decrease.

CE-2 was in an orbit at 100 km above the lunar surface. Each detection area is across about 5° in latitude. Because of the large detection area, the distribution of soil grain size is difficult to accurately estimate. The effect of lunar soil grain size on the calculated results cannot be completely eliminated, but it is partly eliminated by using intensity fraction (ratio of X-ray fluorescence intensity for an element to total intensities of X-ray fluorescence) in this paper.

5.2 Analysis of the difference between results

There are no elemental abundances derived from

other X-ray spectrometers in the region analyzed in this paper. The average elemental abundances of Apollo 11, 12 and Luna 16, 24 samples which came from mare region (McKay et al., 1991; Ouyang Ziyuan et al., 2005) and the results of LP GRS (Prettyman et al., 2006) are listed in Table 4 as references. As shown in Table 4 and Fig. 8, changes in calculated results with latitude during the M solar flare show a similar trend with respect to the results derived from LP GRS. The abundance of Fe derived by CE-2 XRS is high, which is in accordance with the characteristics of mare.

The elemental abundances derived from CE-2 XRS have differences from the LP GRS results and composition of returned samples. The factors giving rise to the differences are presented as follows:

(1) Detection regions are different. There are no returned samples in the observed region by far. Samples were respectively collected by Apollo 11 and 12 in the Tranquillitatis (0°41.4'N, 23°25.8'E) and Oceanus Procellarum (2°27'S, 23°20.4'W), and by Luna 16 and 24 in the Foecunditatis (0°41'S, 56°18'E) and Crisium (12°15'N, 62°12'E). The compositions of these samples are listed in Table 4 as references, but the observed regions in this paper are located in different areas.

(2) Spatial resolution of detection is different. Lunar samples were collected at one point on the surface and they can only represent the region within thousands of square meters of the landing site. The instantaneous detection area of CE-2 XRF on the lunar surface was about 73 km×200 km. Events of X-ray fluorescence in a 100 s period were accumulated in this paper and the corresponding distance of lunar surface is about 150 km (about 5°). LP GRS integrated events of gamma-ray within a 32 s period, and the corresponding footprint is about 50 km.

(3) Detection depths are different. Detection depth of XRF is merely on a micrometer scale. XRF could obtain X-ray fluorescence generated from uppermost soil particles of lunar surface. In contrast, the detection depth of GRS is on a centimeter scale. The returned samples have a certain sampling depth and not all of the samples come from the uppermost layer. Based on the analysis data on Apollo and Luna samples, it is found that the samples of different grain sizes have various compositions, even though they were collected from the same sampling site. The elemental abundances of the particles smaller than 10 μ are significantly different from those of the particles larger in size (Papike et al., 1982; Devine et al., 1982; Laul et al., 1982).

6 Conclusions

In this paper, we have discussed instrument design, data product and the method for analyzing the data of CE-2 XRS. Then, the elemental abundances of Mg, Al, Si, Ca and Fe have been acquired by the inversion method using the data acquired from 9:6:36 to 9:15:46 on Feb. 16, 2011 during the M solar flare. The observation area is located at the Oceanus Procellarum (12.8°–38.2° N, 50° W). The main conclusions are presented as follows:

(1) By comparison with LP GRS results, it is found that the calculated composition is overall higher in Fe, in the region where the latitude is higher than 25° the composition is higher in Al and lower in Ca, while in the region where the latitude is lower than 25° the abundances of Si are higher. But changes in CE-2 XRS results with latitude show a similar trend with respect to the results of LP GRS and the high abundance of Fe is in accordance with the characteristics of lunar mares.

(2) Lunar soil grain size is an important factor which affects the calculated results of XRF data. The effect decreases with the decline of soil grain size. According to previous analysis, most uppermost soil particles of lunar surface are very fine. The detection depth of XRF is merely of micrometer scale, so that the effect of lunar soil grain size is not taken into account in this paper.

(3) We systematically analyzed the factors giving rise to the differences between CE-2 XRS results and LP GRS results as well as the composition of returned samples. They mainly include different detection regions, different spatial resolutions of detection and different detection depths.

Acknowledgements This work was financially supported jointly by the NSFC program(40904051), CAS Program (XDA04071900) and Science and Technology Development Fund in Macao SAR (Grant Number: 048/2012/A2).

References

Adler I., Gerard J., TrombkaJ.I. et al. (1972) The Apollo 15 X-ray fluorescence experiment. In *Proc. Lunar Sci. Conf.* (3rd) [C]. pp.2157–2178.

Adler I., Trombka J.I., Schmadebeck R. et al. (1973a) Results of the Apollo 15 and 16 X-ray experiment. In *Proc. Lunar Sci. Conf.* (4th) [C].pp.2783–2801.

Adler I., Trombka J.I., LowmanP. et al. (1973b) Apollo 15 and 16 results of the integrated geochemical experiment [J]. *The Moon*.**7**, 487–504.

Clark P.E. and Trombka J.I. (1997) Remote X-ray spectrometry for NEAR and future missions: Modeling and analyzing X-ray production from source to surface [J]. *Geophys. Res.***102**, 16361–16384.

Devine J.M., McKay D.S., and Papike J.J. (1982) Lunar regolith: Petrology of the <10 μm fraction [J]. *Geophys. Res.***87**, 260–268.

Ji Ang (2003)*Analysis of X-ray Fluorescence Spectroscopy*[M]. Science

Press, Beijing (in Chinese).

Laul J.C., Papike J.J., and Simon S.B. (1982) The lunar regolith: Comparative studies of Apollo and Luna sites. Chemistry of soils from Apollo 17, Luna 16, 20 and 24. In *Proc. Lunar Planet. Sci. Conf.* (12th) [C]. pp.389–407.Pergamon Press Inc., New York.

Maruyama Y., Ogawa K., Okada T., and Kato M. (2008) Laboratory experiments of particle size effects on X-ray fluorescence and implications to remote X-ray Spectrometry of lunar regolith surface [J]. *Earth Planets Space*.**60**, 293–297.

McKay D.S., Heiken G., Basu A., Blandford G., Simon S., Reedy R., French B.M., and Papike J. (1991)*Lunar Source Book: A User's Guide to the Moon*[M]. Cambridge Univ. Press, Cambridge, England.

Naranen J., Parviainen H., and Muinonen K. (2007) X-ray fluorescence modelling for Solar system regoliths: Effects of viewing geometry, particle size, and surface roughness. In *Proceedings of the 236th IAU Symposium* [C]. pp.43–250.Cambridge University Press.

Naranen J., Parviainen H., Muinonen K., Carpenter J., Nygard K., and Peura M. (2008)Laboratory studies into the effect of regolith on planetary X-ray fluorescence spectroscopy [J]. *Icarus*.**198**, 408–419.

Naranen J., Carpenter J., Parviainen H., Muinonen K., Fraser G., Peura M., and Kallonen A. (2009)Regolith effects in planetary X-ray fluorescence spectroscopy: laboratory studies at 1.7–6.4 keV [J]. *Adv. Space Sci*. **44**, 313–322.

Narendranath S., Athiray P.S.,Sreekumar P. et al. (2011) Lunar X-ray fluorescence observations by the Chandrayaan-1 X-ray Spectrometer (C1XS): Results from the nearside southern highlands [J]. *Icarus*.**214**, 53–66.

Nittler L.R., Starr R.D., Lim L. et al. (2001) X-ray fluorescence measurements of the surface elemental composition of asteroid 433 Eros [J]. *Met. Plan. Sci*. **36**, 1673–1695.

Noble S.K. (2010) Examining the uppermost surface of the lunar regolith. In *Proc. Lunar Planet. Sci. Conf.* (41st) [C].pp.1505.

Okada T. and Kuwada Y. (1997) Effect of surface roughness on X-ray fluorescence emission from planetary surfaces. In *Proc. Lunar Planet. Sci. Conf.* (28th) [C]. pp.1708.

Okada T. (2004) Particle size effect in X-ray fluorescence at a large phase angle: Importance on elemental analysis of asteroid Eros (433). In *Proc. Lunar Planet. Sci. Conf.* (35th) [C].pp.1927.

Okada T., Shiraishi H., Shirai K., Yamamoto Y., Arai T., Ogawa K., Kato M., Grande M., and the Selene XRS Team (2009) X-ray fluorescence spectrometer (XRS) on kaguya: Current status and results. In *Proc. Lunar Planet. Sci. Conf.* (40th) [C].pp.1897.

Ouyang Ziyuan (2005) *Introduction to Lunar Science* [M]. Chinese Aerospace Press, Beijing (in Chinese).

Papike J.J., Simon S.B., White C., and Laul J.C. (1982) The relationship of the lunar regolith <10 μm fraction and agglutinates. In*Proc. Lunar. Planet. Sci. Conf.* (12th) [C].pp.409.

Peng Wenxi (2009)*Data Processing Method Investigation of CHANG'E-1 X-ray Spectrometer* [D].PhD thesis. UCAS.

Prettyman T.H., Jagerty J.J., Elphic R.C., Feldman W.C., Lawrence D.J., Mckinney G.W., and Vaniman D.T. (2006) Elemental composition of the lunar surface: Analysis of gamma ray spectroscopy data from Lunar Prospector[J]. *Geophys. Res*. **111**, 12007–12048.

Sherman J. (1955) The theoretical derivation of fluorescence X-ray intensities from mixtures [J]. *Spectrochim. Acta*.**7**, 283–306.

Shirawai T. and Fujino N. (1966) Theoretical calculation of fluorescent X-ray Intensities in fluorescent X-ray spectrochemical analysis[J]. *Appl. Phys*. **5**, 886–899.